Lagrangian Simulation of a Reacting Mixing Layer at Low Heat Release

Ahmed F. Ghoniem*
Massachusetts Institute of Technology, Cambridge, Massachusetts
and
Peyman Givi†
Flow Research Company, Kent, Washington

The vortex-scalar element method, a Lagrangian scheme which utilizes vortex elements to discretize the vorticity field and scalar elements to represent species or temperature fields, is utilized in the numerical simulation of a two-dimensional, non-premixed, incompressible reacting mixing layer at high Reynolds and Peclet numbers without resorting to turbulence models. In non-reacting flow, conserved scalar mean and fluctuation profiles show good agreement with experimental measurements. In reacting flow, results indicate that for temperature-independent kinetics, the chemical reaction starts immediately downstream of the splitter plate, where mixing starts. With Arrhenius kinetics, ignition delay, which depends on the reactant's temperature, is observed. In this case, strong stretch along the braids may cause local quenching due to the temperature drop associated with large diffusive fluxes. Harmonic forcing changes the layer structure and the mixing rates in accordance with experimental results.

I. Introduction

NON-PREMIXED turbulent reacting flow has been the subject of extensive experimental and theoretical investigations (for review, see Bilger[1]). In most of the theoretical work, turbulence models are used to close a system of averaged transport equations that describe the statistical behavior of the aerothermodynamic variables. Much effort has gone into constructing accurate models and obtaining results that are in agreement with experimental measurements. Moment methods,[2] eddy break-up and mixing controlled models,[3] flame-sheet approximations,[4] assumed probability-density function (PDF) shape methods,[5] and solutions based on modeled joint PDF of scalar quantities[6,7] and based on modeled joint PDF of scalar and velocity[8] are examples of these models.

Recent progress in numerical methods and the availability of fast computers have had a major impact on turbulence research. With more accurate numerics and increased storage and computational speed, it has been possible to solve the time-dependent transport equations governing turbulent combustion over some limited parameter range without the need for modeling. Such nearly model-free "simulations" have the advantage that the physics of the problem is not modeled a priori but is recovered directly from the solution. The results of the simulation can be used to understand important mechanisms of turbulent transport and its influence on chemical reactions. Furthermore, since the instantaneous behavior of the variables is known at all points and at all times, accurate simulations offer a good method of probing the flow. There are still, however, some limitations on the range of turbulent scales that can be resolved accurately by model-free simulations, and there is a need to validate the results of the simulations by direct comparisons with experimenal measurements.

Presented as Paper 87-0225 at the AIAA 25th Aerospace Sciences Meeting, Reno, NV, Jan. 12–15, 1987; received March 25, 1987; revision received Oct. 26, 1987.

*Associate Professor, Department of Mechanical Engineering. Associate Fellow AIAA.
†Research Scientist. Member AIAA.

Numerical methods have been used in a variety of forms for the simulation of turbulent flows in complex configurations (see, e.g., Refs. 9 and 10). Finite-difference methods, in which flow variables are defined on a grid and the transport equations are approximated by discretizing the derivatives on the grid nodes, were first to be used. Examples of this approach can be found in the work of Corcos and Sherman,[11] who used a projection method to study the temporal evolution of a periodic shear layer, and in Grinstein et al.,[12] who used a flux-corrected transport scheme to simulate the development of coherent structures in a two-dimensional, spatially evolving shear layer and examined their effect on mixing.

Spectral methods, in which each variable is expanded in a series of harmonic functions that satisfy the differential equations on a number of collocation points, were applied by Riley et al.[13] to study a three-dimensional temporally evolving reacting mixing layer assuming a constant reaction rate, constant density, and no heat release. McMurtry et al.[14] used a pseudo-spectral scheme to analyze the effect of chemical heat release on the dynamics of a two-dimensional mixing layer for a constant reaction rate. Givi et al.[15] employed a spectral simulation of a two-dimensional mixing layer with an Arrhenius chemical reaction and constant density to study local flame extinction. Extension to spatially growing layers was initiated by Givi and Jou.[16] In all cases, the Reynolds number was kept at order of (100), limited by the grid resolution and the number of harmonic modes.

Vortex methods, in which the transport of the variables takes place in a Lagrangian grid-free form using computational elements that are distributed around regions of strong vorticity, have also been extended to reacting flows. The application of these methods in the calculation of premixed flames has been reported, among others, by Ghoniem et al.[17] and Sethian.[18] In diffusion flames, Ashurst and Barr[19] used the vortex method and an Eulerian flux-corrected transport algorithm to compute the transport of a conserved Shvab-Zeldovich scalar approximating the shape and convolution of the flame in the limit of infinitely fast chemical reaction. Lin and Pratt[20] used the vortex method and a Monte-Carlo method to calculate the time-dependent PDF of the scalar quantities for both gaseous and aqueous mixing layers. The

PDF transport equation required a closure model for the molecular mixing term.

In this work, we extend the vortex method[21] to study non-premixed chemical reactions by employing the scalar element method to treat the scalar field in a Lagrangian form. The fact that a chemical reaction is truly a Lagrangian process, i.e., it occurs when the particles interact as they flow, motivates the implemenation of a Lagrangian method for the simulation of high Reynolds number reacting flows. The method is capable of handling a wide variety of initial and boundary conditions and is not limited to simple flow boundaries. In this paper, we concentrate on the formulation of the model and the numerical schemes, and present some validation studies and interpretations of the results.

II. Formulation and Numerical Scheme

A two-dimensional, confined, planar mixing layer is considered. A schematic diagram for the flowfield is shown in Fig. 1. Two initially unmixed reactants, fuel F and oxidizer O, are present in small concentrations in the top high-speed stream and bottom low-speed stream, respectively. We make the following assumptions: 1) the heat release is low so that its effect on the flow dynamics is negligible; 2) the Mach number is small; 3) the freestream concentrations of F and O are equal and constant; 4) the molecular diffusivities are equal and constant; 5) the viscosity is the same in both streams; and 6) the chemical reaction between F and O is single step, irreversible, and second order. The density is, therefore, constant, and the transport equations of the hydrodynamic field and the scalar—temperature or species—fields are decoupled. The equations governing this system are

$$F+O \xrightarrow{k} P \tag{1}$$

$$\nabla^2\psi = -\omega(x,t) \tag{2}$$

$$\frac{\partial\omega}{\partial t}+u\cdot\nabla\omega=\frac{1}{R_e}\nabla^2\omega \tag{3}$$

$$\frac{\partial T}{\partial t}+u\cdot\nabla T=\frac{1}{P_e}\nabla^2 T+QD_a\dot{W} \tag{4}$$

$$\frac{\partial c_j}{\partial t}+u\cdot\nabla c_j=\frac{1}{P_eL_e}\nabla^2 c_j-D_a\dot{W} \tag{5}$$

$$\frac{\partial c_p}{\partial t}+u\cdot\nabla c_p=\frac{1}{P_eL_e}\nabla^2 c_p-D_a\dot{W} \tag{6}$$

where P indicates products; $\dot{W}=c_Fc_0\exp(-T_a/T)$ is the reaction rate, written in terms of the rate of generation of products per unit mass; $u=(u,v)$ is the velocity; $x=(x,y)$ where x,y are the streamwise and cross-stream directions, respectively; t is time; ψ is the stream function defined such that $u=\partial\psi/\partial y$ and $v=-\partial\psi/\partial x$; $\omega=\nabla xu$ is the vorticity; c is the concentration per unit mass; T is temperature; $\nabla=(\partial/\partial x,\ \partial/\partial y)$; and $\nabla^2=\partial^2/\partial x^2+\partial^2/\partial y^2$. Variables are non-dimensionalized with respect to the appropriate combination of the velocity difference, $\Delta U=U1-U2$; the channel height, H; the freestream concentration of F, c_{Fo}, and the freestream temperature at $x=0$, T_0. In Eq. (5), $j=F$ or O for fuel and oxidizer, respectively. $R_e=\Delta U\,H/\nu$ is the Reynolds number, where ν is the kinematic viscosity. The reaction rate constant $k=A\exp(-T_a/T)$ where A is the frequency factor non-dimensionalized with respect to (RT_0), T_a is the activation energy, and R is the gas constant. The enthalpy of reaction, non-dimensionalized with respect to C_pT_0 is Q, where C_p is the specific heat at constant pressure. The Peclet number is $P_e=\Delta U\,H/\alpha$, where α is the thermal diffusivity. The first Damkohler number is $D_a=Ac_{Fo}^2\,H/\Delta U$, where D is diffusivity, and $L_e=\alpha/D$ is the Lewis number.

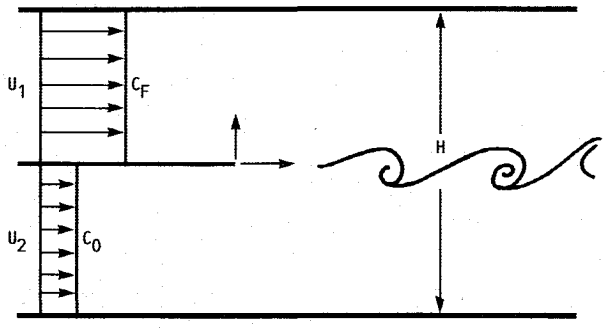

Fig. 1 Schematic diagram of the shear layer model.

Vortex Scheme

A complete description of the vortex method as applied to the present problem is given by Ghoniem and Ng[21] and is briefly described here. The vorticity field is represented by a finite number of vortex elements that possess finite cores:

$$\omega(x,t)=\frac{\Gamma_i}{\delta^2}f(x-\chi_i) \tag{7}$$

where $\Gamma_i=\int\omega\,dA$ is the circulation of a vortex element, δ is the core radius, χ_i is the center of the element, and f represents the vorticity distribution associated with a vortex element or the core function (Chorin,[22] Hald,[23] Beale and Majda,[24] and Ghoniem and Gagnon[25]). The velocity field is obtained by solving Eq. (2) using the discrete vorticity distribution and satisfying the potential condition on the boundaries of the domain. In this work, we use Rankine vortex elements, i.e., $f(r)=1/\pi$ for $r\le\delta$ and $f(r)=0$ for $r>\delta$.

The motion of the vortex elements is constructed such that the discrete vorticity field approximates Eq. (3). This is accomplished by solving this equation in two fractional steps. In the first step, convective transport is implemented in terms of the Lagrangian displacement of vortex elements using the velocity field. In the second step, the solution of the diffusion equation is simulated stochastically by the random walk of the vortex elements according to the appropriate population. The no-slip boundary condition at the walls is satisfied by generating new vortex elements to cancel the velocity induced by the vorticity field. Here, we generate vorticity only at the point of separation, i.e., at the tip of the splitter plate, since the growth of the boundary layers along the channel walls at high Reynolds numbers is small. At each time step, the new vorticity $\Delta\Gamma=-\Delta U\,U_m\Delta t$, where $U_m=(U1+U2)/2$, is assigned to N_o elements of strength $\Delta\Gamma/N_o$ and added to the field at points $\Delta x=U_m\Delta t/N_o$ apart downstream of $x=0$.

The effect of the numerical parameters on the accuracy of the results was investigated by Ghoniem and Ng.[21] Their results indicate that $N_o=6$ is necessary to obtain well-defined eddy structures after the roll-up and the first pairing. The second pairing occurs within the domain of $0\le x\le 6$; therefore, the computational domain was limited to $x_{\max}=6$. Downstream of $x_{\max}$, the vorticity was deleted. Varying $x_{\max}$ showed that the effect of deleting the vortex elements propagates about one channel height upstream, hence the results are accurate only for $0\le x\le 5$.

Scalar-Element Method

In this scheme, which is a two-dimensional extension of the random element method of Ghoniem and Oppenheim,[26] the scalar field is represented by a set of elements, each carrying a finite amount of the scalar field:

$$s(x,t)=\sum\delta s_i\,\delta(x-\chi_i) \tag{8}$$

where s is a scalar, i.e., the temperature or species concentration δs_i is the strength of an element defined as the amount of scalar carried by this element, and $\delta(\cdot)$ is the Dirac delta function. The element strength $\delta s_i = 1/\delta A \int s(x,t)\, dA$, where $\delta A = \delta x \delta y$, and δx and δy are the distances between the centers of neighboring elements in the streamwise and cross-stream directions, respectively, and χ_i is the center of the element. If s is a reacting scalar, its transport is governed by

$$\frac{\partial s}{\partial t} + u \cdot \nabla s = \frac{1}{S_e} \nabla^2 s + D_s \dot{W} \tag{9}$$

where S_e is the ratio between the diffusive and convective transport time scales of s, $S_e = P_e$ for T, and $S_e = P_e L_e$ of c, while $D_s = QD_a$ for T, $D_s = -D_a$ for c_F and c_0, and $D_s = D_a$ for c_p. In the scalar-element method, this equation is solved in three fractional steps:

Convection:

$$\frac{\partial s}{\partial t} + u \cdot \nabla s = 0 \tag{10}$$

Diffusion:

$$\frac{\partial s}{\partial t} = \frac{1}{S_e} \nabla^2 s \tag{11}$$

Reaction:

$$\frac{\partial s}{\partial t} = D_s \dot{W} \tag{12}$$

Convective and diffusive transport are performed in a similar way as in the vortex method, i.e., by the Lagrangian motion of the scalar elements using the velocity field u, and the random walk of the elements using a set of Gaussian random variables with zero mean and standard deviation $\sqrt{2\Delta t/S_e}$ (Ghoniem and Sherman[27]). If χ_i is the center of the element i, and Σ_k stands for a multistep integration scheme, then

$$\chi_i(t+\Delta t) = \chi_i(t) + \Sigma_k u(\chi_{ik}) \Delta t + \eta_i \tag{13}$$

Chemical reaction changes the amount of scalar carried by the element according to the integration of Eq. (12),

$$\delta s_i(t+\Delta t) = \delta s_i(t) + D_s \dot{W} \Delta t \tag{14}$$

However, the reaction occurs only when the elements are close enough for molecular mixing to affect their composition. Therefore, at every time step, the distance between the centers of each two elements of F and O $\Delta\chi_{ij} = |\chi_i - \chi_j|$ is computed. If $\Delta\chi_{ij} \leq \delta_D$, where $\delta_D = 0(1/\sqrt{S_e})$ is the diffusion length scale, the composition of each of the two elements changes according to Eq. (14). The initial distance between neighboring elements must be small enough to allow interactions between the elements.

III. Results and Discussion

Nonreacting Mixing Layer

Results of a typical simulation, presented in terms of the velocity and location of all vortex elements used in the computations, is shown in Fig. 2 for $R_e = 10{,}000$, and $U1/U2 = 1/2$. Each element is depicted as a point, while its velocity relative to the mean velocity is represented by a line vector starting at the center of the element. Results show the formation of large eddies by the roll-up of the vorticity layer that emanates at the splitter plate, and the subsequent pairing of these eddies into larger structures. These dynamics were investigated in Ghoniem and Ng[21] by analyzing results at a wide range of Reynolds number with different boundary conditions. Their conclusions can be summarized as follows: 1) the roll-up is due to the growth of perturbations by the Kelvin–Helmholtz instability, and the shedding frequency corresponds to the most unstable frequency predicted by the linear stability analysis of a spatially growing layer; 2) pairing, which is associated with the local subharmonic perturbations, results in a stepwise increase in the size of the vorticity layer as two eddies merge; 3) the two sources of the subharmonic perturbations are the downward motion of the layer and the monotonic growth of the eddies downstream; and 4) the computed velocity statistics show good agreement with experimental data, indicating that the fundamental mechanisms of the shear layer in the initial stages are two-dimensional.

To study entrainment, a passive conserved scalar with a normalized concentration $c = 0$ in the high-speed stream and $c = 1$ in the low-speed stream is introduced at the inlet section. At each time step, 19 elements are introduced in each stream, with strength $\delta c = 0$ for $y \geq 0$ and $\delta c = 1$ for $y < 0$. The initial distances between two neighboring elements are $\delta x = 0.075$, since $\delta t = 0.1$, and $\delta y = 0.021$. Since diffusion is more critical in the cross-stream direction, δy is chosen to be smaller than δx. A case with $\delta y = 0.016$, using 25 elements in each stream, was computed showing no significant change in the results. Figure 3 exhibits the strength of each of the scalar elements at $t = 28$, 29, and 30. In this figure, the dots represent the fluid from the high-speed stream, $c = 0$; and the open circles represent the fluid from the low-speed stream, $c = 1$. The results indicate that the large eddies entrain fluid from both sides of the freestreams into the cores of the vorticity layer, which leads to the enhancement of mixing between the two streams. Entrain-

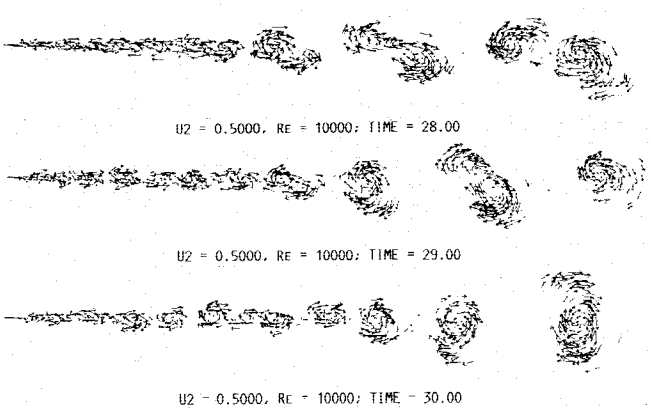

Fig. 2 Vortex elements and their velocity vectors at $R_e = 10{,}000$, $U1/U2 = 2$.

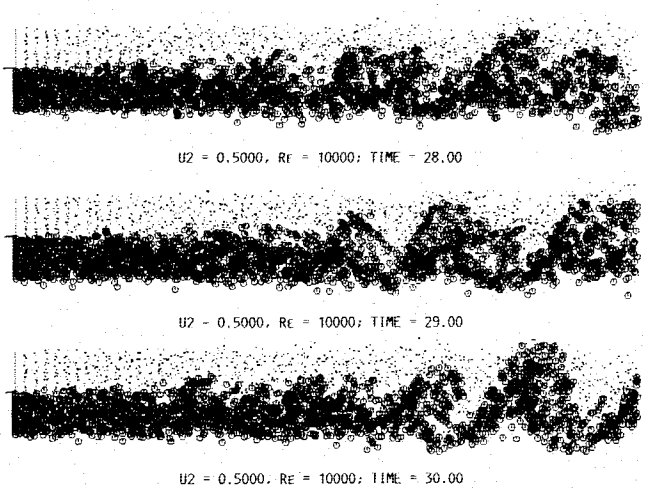

Fig. 3 Concentration field at $R_e = 10{,}000$, $P_e = 4000$, $U2/U1 = 0.5$.

ment asymmetry is observed as more fluid from the high-speed side is drawn into the low-speed side (Koochesfahani[28]).

Time-averaged statistics of the scalar concentration are compared with experimental data in Figs. 4 and 5. Since the time-dependent evolution of a spatially inhomogeneous flow is computed, spatial and temporal averagings are necessary to evaluate these statistics. The instantaneous concentration at a point is computed by averaging the strength of the scalar elements occupying one grid cell $(\Delta x, \Delta y)$ around this point. The size of this cell is chosen to be larger than the average distance between two neighboring elements to ensure that more than one element represents the local concentration, but smaller than the scale of a large structure to guarantee fine spatial resolution. The instantaneous concentration is then averaged over a time period longer than the longest flow time scale to compute the mean and the fluctuations. Another method of computing these statistics is to count the total number of elements that pass through a cell over this period of time and then use this ensemble of elements to perform the statistics. If M elements, with strength δc_i, flow through a cell within a period of time $t = k\Delta t$ then

$$\bar{c} = \frac{1}{M} \sum_{i=1}^{M} \delta c_i$$

and

$$\overline{c'^2} = \frac{1}{M} \sum_{j=1}^{K} M_j (\bar{c} - \overline{\delta c_j})^2$$

while

$$M = \sum_{j=1}^{K} M_j, \qquad \overline{\delta c_j} = \frac{1}{M} \sum_{i=1}^{M_j} \delta c_i$$

where M_j is the number of elements in a cell at a paricular time step. Although the two methods of averaging are equivalent when the number of elements is large, the second scheme converges faster.

To obtain the results in Figs. 4 and 5, we used $\Delta x = 0.1$, $\Delta y = 0.03$, and $K = 160$ time steps after the flow had reached a stationary state, with $16 \le t \le 32$. Within this period, more than 20 large eddies passed through a streamwise location, and an ensemble of $M = 200$ were collected in each cell, depending on the cross-stream location. Figure 4 shows the mean concentration $\bar{c}$ as a function of the reduced coordinate $(y - y_o)/(x - x_o)$, where y_o is measured at $\bar{c} = 0.5$ and x_o is the virtual origin of the mixing layer based on the mean concentration profile (in the calculation, $x_o = 0$). In this figure, the solid line is the computed mean concentration at $x = 4$, and the data points are obtained from the experimental measurements of Masutani and Bowman[29] for a dilute non-reacting mixing layer with the same velocity ratio. Figure 5 shows a comparison between the computed and measured mean fluctuations of the concentration, $\overline{c'^2} = \overline{(c - \bar{c})^2}$. It is evident from the two figures that both the mean and the second moment of the conserved scalar are accurately predicted across the width of the shear layer, except at the edge near the high-speed side. Near this edge, our computations underpredict the concentration statistics due to the lack of scalar elements in the cross-stream direction at $x = 0$. Increasing the number of elements at the boundary is expected to result in better predictions.

It should be noted that the results in Figs. 4 and 5 are in better agreement with experimental data than those obtained by Givi et al.[30] who used a k-ϵ turbulence model and a gradient diffusion model for turbulent transport of the scalar mean, moment, and probability density function. In the k-ϵ calculations, the concentration fluctuations exhibit a fairly smooth bell-shaped profile with a single maximum in the middle region. Our calculations show the presence of two local maxima in the fluctuation profiles that correspond to the locations where the gradient of the mean value is highest, as observed in the experimental results of Masutani and Bowman[29] and Batt.[31] It is clear, in accordance with the findings of Broadwell and Breidenthal,[32] that the intermittency caused by the large coherent structures contributes greatly to the statistics of this turbulent flow.

Reacting Mixing Layer

In the reacting mixing layer calculations, two reactants F and O are introduced on both sides of the splitter plate. At $x = 0$, for $y > 0$, $c_F = 1$, $c_O = 0$, and $c_P = 0$, while for $y < 0$, $c_O = 1$, $c_F = 0$, and $c_P = 0$. As reactants are entrained into the mixing cores of the layer, they diffuse across the original interface and chemical reaction proceeds. The roll-up and pairing stretch the original interface between the streams by many folds, allowing the entrained fluid to diffuse along a larger surface (Ghoniem et al.[33]). During this process, if the Lagrangian elements used to represent the interaction between chemically reacting species are brought close enough so that the distance between two neighboring elements is smaller than the diffusion length scale, they react at the rate defined by Eq. (12).

In Fig. 6, the location and velocity of the scalar elements are shown. The amount of products formed due to chemical reaction is represented by the diameter of the circles in Figs. 7 and 8 for reacting mixing layers with constant-rate chemical kinetics and temperature-dependent reaction rate, respectively, with larger circles indicating more products. In both cases, $R_e = 10{,}000$, $P_e = 4000$, $U1/U2 = 1/3$, and $L_e = 1$. In the constant-rate kinetics $D_a = 1$, whereas in the temperature-

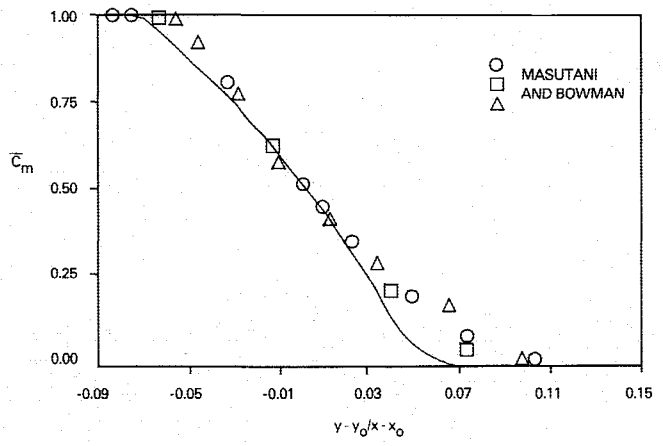

Fig. 4 Normalized mean concentration profile as a function of the cross-stream coordinate.

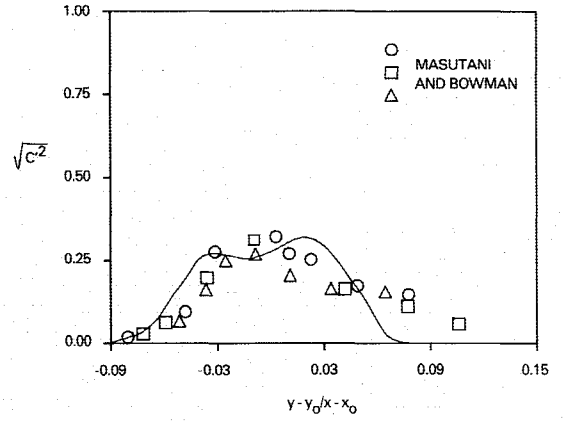

Fig. 5 Normalized concentration fluctuation profile as a function of the cross-stream coordinate.

dependent kinetics $D_a = 200$, $T_a = 10$, and $Q = 5$. Note that, in both cases, the value of the non-dimensional kinetic parameters are low enough so that the effect of heat release on the fluid dynamics can be neglected. The stiffness of Eq. (12) for large values of the Damkohler number imposes a restriction on the time step of integration. In these calculations, we found that $\Delta t = 0.1$ is sufficiently small to integrate accurately the slow chemistry.

A comparison between the two figures reveals that, in the temperature-independent kinetics case, products are formed as mixing starts immediately downstream of the splitter plate. However, in the temperature-dependent kinetics calculations, there is an ignition delay before the reactants reach a temperature high enough to allow any significant chemical reaction to occur. Once the reaction begins, the mechanisms of product formation and chemical reaction in both cases are asymptotically the same. Increasing D_a to 400 results in a shorter ignition delay, and preheating the reactants to $T_i = Q/2$ with $D_a = 200$ eliminates the ignition delay, as indicated in Figs. 9 and 10, respectively.

To examine the effect of chemical reaction on the transport of species, the concentration statistics in the temperature-independent reaction case are plotted in Figs. 11 and 12. These figures correspond to the time-averaged mean and fluctuation in the bottom-stream species concentration in a reacting mixing layer with $D_a = 1$, $U1/U2 = 1/2$, $R_e = 10{,}000$, and $P_e = 4000$. A comparison between Figs. 11 and 4 and between Figs. 12 and 5 indicates that near the freestream, the chemistry does not affect the statistics of the species. Near the reaction zone, however, the mean and fluctuations of the concentration are lower under reacting conditions, while the second hump near the high-speed side of the fluctuations profile in the non-reacting layer is eliminated in the reacting flow due to the local consumption of species by chemical reaction. The same behavior was also observed in the experiment of Masutani and Bowman.[29] Their results, however, cannot be compared quantitatively with the present calculations since the values of the chemical parameters employed in the numerical simulation are substantially lower than those of the experiment.

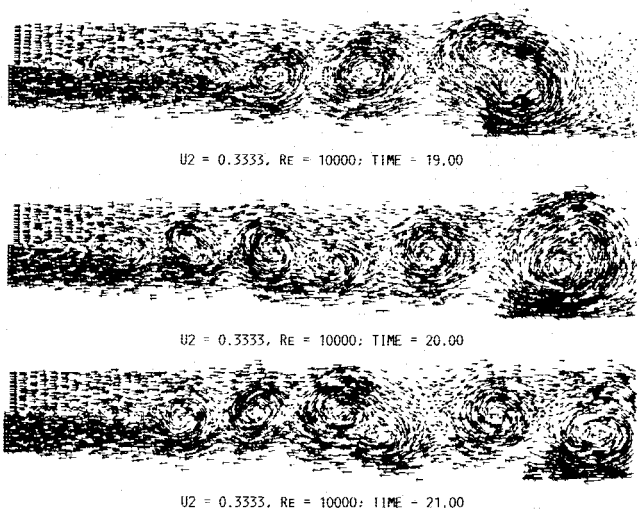

Fig. 6 Velocity and location of the scalar elements at $R_e = 10{,}000$, $U2/U1 = 1/3$.

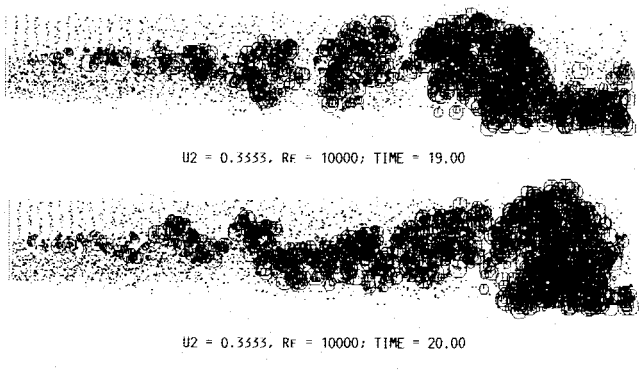

Fig. 7 Product concentration field, $R_e = 10{,}000$, $P_e = 4000$, $U2/U1 = 1/3$, isothermal reacting layer.

Effect of Harmonic Forcing

The dynamic effect of oscillating the upstream side of the layer was studied experimentally by, e.g., Oster and Wygnanski[34] and Roberts and Roshko,[35] and numerically by Ghoniem and Ng.[21] Their results indicate that periodic forcing changes the layer structure as follows: 1) initially, roll-up occurs at the harmonic of the forcing frequency closest to the most ampli-

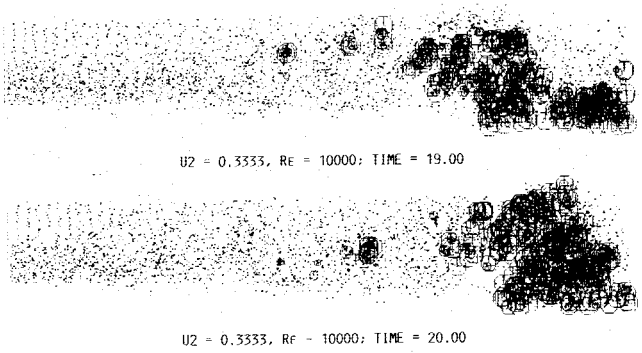

Fig. 8 Product concentration field, variable-temperature reacting layer, $D_a = 1$.

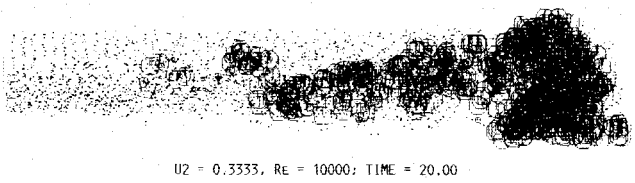

Fig. 9 Product concentration field, variable-temperature reacting layer, $D_a = 400$.

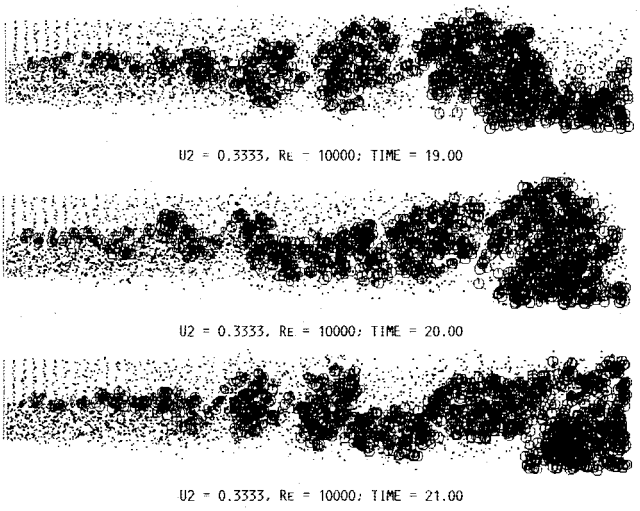

Fig. 10 Product concentration field, variable-temperature reacting layer, $T_i = Q/2$.

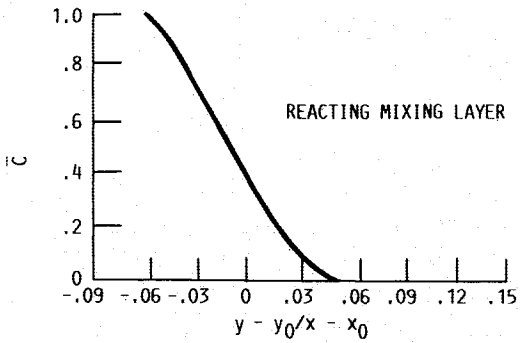

Fig. 11 Normalized mean concentration profile as a function of the cross-stream coordinate.

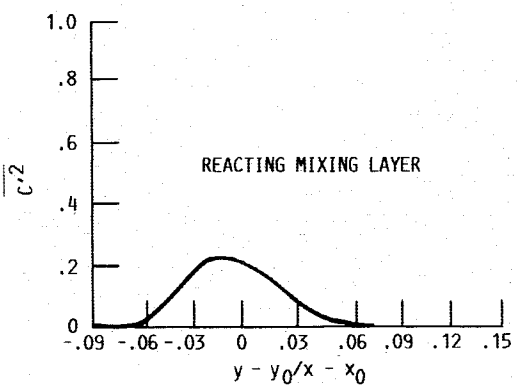

Fig. 12 Normalized concentration fluctuation profile as a function of the cross-stream coordinate.

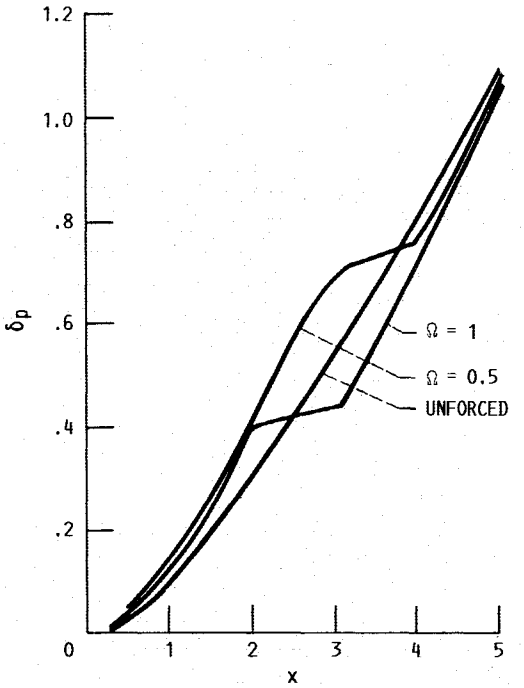

Fig. 13 Variation of the product thickness vs the downstream distance.

Table 1 Comparison between calculated and measured frequency-locked region

	Frequency-locked region	
Ω	Calculated	Measured[36]
0.5	$3 \le x \le 4$	$2.66 \le x \le 5.33$
1.0	$2 \le x \le 3$	$1.33 \le x \le 2.66$

fied frequency and pairing is accelerated until a resonant eddy, which is in tune with the forcing frequency, is formed; 2) pairing among resonant eddies is disabled and the growth of the vorticity layer is impaired for several eddies downstream; and 3) finally, pseudorandom pairing is resumed. Velocity statistics are affected by forcing, and the sign of momentum transfer across the layer is reversed following pairing. Entrainment of passive particles was found to be commensurate with the development of the vorticity layer.

The effect of periodic forcing on mixing and chemical reaction across a shear layer was observed in the experiment by Roberts and Roshko.[35] Their results show that when periodic forcing is applied, the mixing rate 1) is increased in the initial stages where the resonant eddy is forming; 2) is decreased in the intermediate stage that corresponds to the "frequency-locked" region; and 3) is the same as that of the unforced layer further downstream. The Wygnanski-Oster parameter, $X_w = \Delta U \Omega x / U_m^2$, where Ω is the forcing frequency, can be used to define the extent of each region. Roberts and Roshko[35] and Browand and Ho[36] showed that $X_w < 1$ corresponds to the first region where the growth rate is enhanced; $X_w > 1$ begins the frequency-locked region in which the growth is inhibited; and around $X_w \approx 2$ the layer relaxes to the natural growth of an unforced flow.

In order to investigate this phenomenon computationally, the response of the reacting shear layer to the application of low frequency, low-amplitude perturbations on the upstream side of the shear layer is analyzed. Streamwise oscillations are applied on both sides of the layer, hence a pressure perturbation is imposed without changing the vorticity field. The streamwise velocities are taken as $U1 = 1 + a \sin(2\pi\Omega t)$, and $U2 = \alpha U1$, where a is the amplitude of forcing.

The normalized distribution of the product thickness along the mixing layer for three cases, $\Omega = 0$, 0.5, and 1, is shown in Fig. 13. In these calculations, $a = 0.1$ and $R_e = 4000$. The figure indicates that for $\Omega = 1$, mixing is enhanced in the initial part of the layer with $1 \le x \le 2$. The resonant, frequency-locked region begins at $x = 2$ and ends at value $x \sim 3$. In this region, mixing is reduced and is less than that of an unforced mixing layer. Downstream of this region, $x \ge 3$, the mixing rate resumes its natural growth and reaches asymptotically that of the unforced layer. For a lower forcing frequency, $\Omega = 0.5$, the same overall behavior is observed. In this case, however, the results of the numerical calculations indicate that the resonant, frequency-locked region is approximately in the range $3 \le x \le 4$. A comparison between the calculated range of the frequency-locked region and that estimated by Browand and Ho[36] is shown in Table 1.

Effect of Strain Rate

It has been shown experimentally by Tsuji,[37] numerically by Liew et al.,[38] and analytically by Peters[39] that the strain rate has a major influence on the structure of non-premixed flames. In the counterflow diffusion flame experiment of Tsuji,[37] it was observed that increasing the magnitude of stretch near the flame surface results in an increase of the flow of reactants into the reaction zone. As a result, the chemical reaction is not able to keep pace with the supply of reactants, and the reaction rate is reduced until local flame quenching occurs. The analysis of Peters,[39] which is based on the method of matched asymptotic expansion at large activation energy, shows that the mechanism of flame extinction can be addressed by examining the local value of the rate of scalar dissipation, which is the inverse of the diffusion time scale. If the local value of dissipation is increased beyond a critical limit, the heat conducted away from the flame cannot be balanced

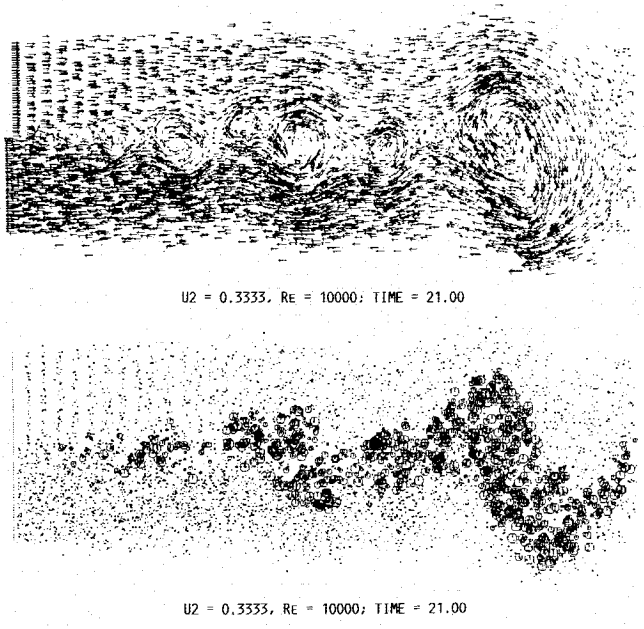

Fig. 14 Velocity of elements and temperature field for reacting mixing layer.

by the heat produced by the chemical reaction. As a result, the maximum value of the temperature decreases, and the reaction eventually ceases.

We were able to observe this phenomenon by increasing the number of scalar elements to 38 in each stream while decreasing the computational domain to $x_{max}=4$ and by preheating the incoming reactants to $T_i=Q/2$ to start the chemical reaction immediately downstream of the splitter plate. Figure 14 shows the instantaneous velocity and temperature rise, $T-T_i$, of the scalar elements at time $t=21$, for $D_a=50$, $Q=8$, $T_a=20$, and $U1/U2=1/3$. The cross-stream direction is enlarged by a factor of two for the purpose of clarity. The figure shows that the number of scalar elements near the braid, which is the thin link between two neighboring cores, is a small portion of the total number of elements within the computational domain, which reached more than 5100. The temperature and product concentration in the reaction zone reach a maximum at the eddy cores where the vorticity concentration is high, while they reach a minimum at the stagnation point within the braids where the strain and the scalar gradient reach their maximum values. This is consistent with the results of the pseudospectral calculation of Givi et al.[15] and with the experimental observations of Tsuji,[37] who showed that the local extinction of diffusion flames occurs mainly at the regions of high dissipation rate. In these regions, the temperature tends to decrease, and if it goes below a critical characteristic value, the flame extinguishes locally.

Quantitative analysis of the effect of stretch on the chemical reaction is difficult in the context of the present algorithm. This is due to the fact that there are few scalar elements near the regions of high strain, and, as shown by Ghoniem et al.,[33] most of the elements tend to agglomorate near the regions with low dissipation. Implementation of a numerical scheme based on the transport of scalar gradient, as in Ghoniem et al.[33] can improve the accuracy of the analysis, particularly those associated with the effects of stretch.

IV. Conclusions

In this work, a stochastic numerical scheme based on the transport of computational elements carrying vorticity and scalar quantities has been developed to simulate a two-dimensional, planar, two-stream reacting mixing layer with unmixed reactants. The scheme solves the transport equations at high Reynolds and Peclet numbers without using models for turbulence closure. A Lagrangian stochastic model is used to implement the chemical reactions for both constant-rate kinetics and variable-temperature Arrhenius reactions, at low heat release.

In the non-reacting flow simulations, the calculated statistics of the mixing of a conserved scalar are in good agreement with experimental data. In particular, the numerical results show the presence of two maxima in the fluctuation profile. In the constant-rate reacting flow simulation, the effect of chemistry is to smooth out this curve and produce a single maximum, which agrees with the experimental observations. Harmonic forcing enhances the mixing within the accelerated growth zone of the vorticity layer, while it impairs the entrainment of the unmixed fluid into the cores in the resonance region. As a result, the numerical simulation indicates a decrease in the rate of product formation in the frequency-locked region, similar to previous experimental findings.

In the Arrhenius, temperature-dependent kinetics, the mechanism of ignition delay and the effect of preheating the reactants on the decrease of the duration of this delay is observed. The non-equilibrium coupling between the scalar dissipation rate and the flame structure is exhibited in the form of quenching, which is frequently observed along the braids. To describe this phenomenon more accurately, work is underway to construct a higher-order scheme which can provide better resolution in the regions of strong strain rates.

Acknowledgments

The work of A.F. Ghoniem is supported by the Air Force Office of Scientific Research Grant AFOSR 84-0356, the National Science Foundation Grant CPE-840481, and the Edgerton Associate Professorship at MIT. Part of this work was performed while P. Givi was on leave at the Institute for Computational Mechanics in Propulsion at NASA Lewis Research Center. The authors appreciate the support of NASA Lewis Research Center in providing computer time on the CRAY-XMP. The help of Mr. Don Lovell of Flow Research Company in vectorizing the codes and in providing graphics routines is gratefully acknowledged.

References

[1]Bilger, R. W., "Turbulent Flows with Non-Premixed Reactants," *Turbulent Reacting Flows*, Springer-Verlag, Berlin, 1980, pp. 65–113.

[2]Donaldson, C. duP. and Varma, A. K., "Remarks on the Constructions of a Second-Order Closure Description of Turbulent Reacting Flows," *Combustion Science and Technology,* Vol. 13, 1976, pp. 55–78.

[3]Givi, P., Ramos, J. I., and Sirignano, W.A., "Turbulent Reacting Concentric Jets: Comparison Between PDF and Moment Calculations," *Progress on Astronautics and Aeronautics,* Vol. 95, AIAA, New York, 1984, pp. 384–448.

[4]Bilger, R. W., "Turbulent Jet Diffusion Flames," *Progress in Energy and Combustion Science,* Vol. 1, 1976, pp. 87–109.

[5]Lockwood, F. C. and Naguib, A.S., "The Prediction of the Fluctuations in the Properties of Free, Round Jet, Turbulent, Diffusion Flames," *Combustion Flame,* Vol. 24, 1975, pp. 109–124.

[6]Givi, P., Sirignano, W. A., and Pope, S.B., "Probability Calculations for Turbulent Jet Flows with Mixing and Reaction of NO and O_3;" *Combustion Science and Technology,* Vol. 37, 1984, pp. 599–674.

[7]Nguyen, T. V. and Pope, S. B., "Monte-Carlo Calculations of Turbulent Diffusion Flames," *Combustion Science and Technology,* Vol. 42, 1984, pp. 13–45.

[8]Pope, S. B. and Correa, S. M., "Joint PDF Calculations of a Non-Equilibrium Diffusion Flame," *Proceedings of the 21st Symposium (International) on Combustion,* The Combustion Institute, Pittsburgh, PA, 1988, pp. 1341–1348.

[9]Ghoniem, A. F., "Computational Methods in Turbulent Reacting Flows," *Lectures in Applied Mathematics,* Vol. 24, American Mathematical Society, Providence, RI, 1986, pp. 199–265.

[10]Oran, E. S. and Boris, J. P., *Numerical Simulation of Reactive Flows,* Elsevier Science Publishing Co., New York, 1987, p. xxi+601.

[11]Corcos, G. M. and Sherman, F. S., "The Mixing Layer: Deterministic Models of a Turbulent Flow; Part 1: Introduction and the Two-Dimensional Flow," *Journal of Fluid Mechanics,* Vol. 139, 1984, pp. 29-65.

[12]Grinstein, F. F., Oran, E. S., and Boris, J. P., "Numerical Simulations of Asymmetric Mixing in Planar Shear Flows," *Journal of Fluid Mechanics,* Vol. 165, 1986, pp. 201-220.

[13]Riley, J. J., Metcalfe, R. W., and Orszag, S.A., "Direct Numerical Simulations of Chemically Reacting Turbulent Mixing Layers," *Physics of Fluids,* Vol. 29, 1986, pp. 406-422.

[14]McMurtry, P. A., Jou, W. H., Riley, J.J., and Metcalfe, R.W., "Direct Numerical Simulations of a Reacting Mixing Layer with Chemical Heat Release," *AIAA Journal,* Vol. 24, June 1986, pp. 962-970.

[15]Givi, P., Jou, W. H., and Metcalfe, R.W., "Flame Extinction in a Temporally Evolving Mixing Layer," *Proceedings of the 21st Symposium (International) on Combustion,* The Combustion Institute, Pittsburgh, PA, 1988, pp. 1251-1262.

[16]Givi, P. and Jou, W. H., "Mixing and Chemical Reaction in a Spatially Developing Mixing Layer," *Journal of Nonequilibrium Thermodynamics,* (to be published).

[17]Ghoniem, A. F., Chorin, A. J., and Oppenheim, A.K., "Numerical Modeling of Turbulent Flow in a Combustion Tunnel," *Philosophical Transactions of the Royal Society of London,* Vol. A304, 1982, pp. 303-325.

[18]Sethian, J. A., "Turbulent Combustion in Open and Closed Vessels," *Journal of Computational Physics,* Vol. 54, 3, 1984, pp. 425-456.

[19]Ashurst, W. T. and Barr, P. K., "Lagrangian-Eulerian Calculation of Turbulent Diffusion Flame Propagation," Sandia National Laboratories, Livermore, CA, Sandia Rept. SAND80-9950, 1982.

[20]Lin, P. and Pratt, D. T., "Numerical Simulation of a Plane Mixing Layer, with Applications to Isothermal, Rapid Reactions," AIAA Paper 87-0224, Jan. 1988.

[21]Ghoniem, A. F. and Ng, K. K., "Numerical Study of a Forced Shear Layer," *Physics of Fluids,* Vol. 30, 1987, pp. 706-721.

[22]Chorin, A. J., "Numerical Study of Slightly Viscous Flow," *Journal of Fluid Mechanics,* Vol. 57, 1973, pp. 785-796.

[23]Hald, O., "The Convergence of Vortex Methods," *SIAM Journal of Numerical Analysis,* Vol. 22, 1979, pp. 726-755.

[24]Beale, J. T. and Majda, A., "Vortex Methods II: Higher-Order Accuracy in Two and Three Dimensions," *Mathematical Computations,* Vol. 39, 1982, pp. 29-52.

[25]Ghoniem A. F. and Gagnon, Y., "Vortex Simulation of Recirculating Flow at Moderate Reynolds Numbers," *Journal of Computational Physics,* Vol. 68, 1987, pp. 346-377.

[26]Ghoniem, A. F. and Oppenheim, A. K., "Numerical Solution of the Problem of Flame Propagation by the Use of the Random Element Method," *AIAA Journal,* Vol. 22, 1984, pp. 1429-1435.

[27]Ghoniem, A. F. and Sherman, F. S., "Grid-Free Simulation of Diffusion Using Random Walk," *Journal of Computational Physics,* Vol. 61, Nov. 1985, pp. 1-37.

[28]Koochesfahani, M. M., "Experiments on Turbulent Mixing and Chemical Reactions in a Liquid Mixing Layer," Ph.D. Thesis, California Inst. of Technology, Pasadena, CA, 1984.

[29]Masutani, S. M. and Bowman, C. T., "The Structure of a Chemically Reacting Plane Mixing Layer," *Journal of Fluid Mechanics,* Vol. 172, 1986, pp. 93-126.

[30]Givi, P., Ramos, J. I., and Sirignano, W.A., "Probability Density Function Calculations in Turbulent, Chemically Reacting Round Jets, Mixing Layers, and One-Dimensional Reactors," *Journal of Nonequilibrium Thermodynamics,* Vol. 10, 1985, pp. 75-104.

[31]Batt, R. G., "Turbulent Mixing of Passive and Chemically Reacting Species in a Low-Speed Shear Layer," *Journal of Fluid Mechanics,* Vol. 82, 1977, pp 53-95.

[32]Broadwell, J. E. and Breidenthal, R.E., "A Simple Model of Mixing and Chemical Reaction in a Turbulent Shear Layer," *Journal of Fluid Mechanics,* Vol. 125, 1982, pp. 397-410.

[33]Ghoniem, A. F., Heidarinejad G., and Krishnan, A., "Numerical Simulation of a Thermally Stratified Mixing Layer Using the Vortex Element Method," *Journal of Computational Physics,* (to be published).

[34]Oster, D. and Wygnanski, I., "The Forced Mixing Layer Between Parallel Streams," *Journal of Fluid Mechanics,* Vol. 123, 1982, pp. 91-130.

[35]Roberts, R. A. and Roshko, A., "Effects of Periodic Forcing on Mixing in Turbulent Shear Layers and Wakes," AIAA Paper 85-0570, March 1985.

[36]Browand, F. E. and Ho, C. M., "The Mixing Layer: An Example of Quasi Two-Dimensional Turbulence," *Journal de Mecanique Theorique et Appliquee Numero Special,* 1983, pp. 99-120.

[37]Tsuji, H., "Counter-Flow Diffusion Flames," *Progress in Energy Combustion Science,* Vol. 8, 1982, p. 93.

[38]Liew, S. K., Moss, J. B., and Bray, K.N.C., "Predicted Structure of Stretched and Unstretched Methane-Air Diffusion Flame," *Progress in Astronautics and Aeronautics,* Vol. 95, AIAA, New York, 1984, pp. 305-319.

[39]Peters, N., "Laminar Diffusion Flamelets Models in Non-Premixed Turbulent Combustion," *Progress in Energy Combustion Science,* Vol. 10, 1984, pp. 319-339.